Journal of Nuclear Medicine, published on January 26, 2023 as doi:10.2967/jnumed.122.264552

Radiolabeled GPVI-Fc for PET imaging of multiple extracellular matrix fibers: A new look into pulmonary fibrosis progression.

Simon Isser[1], Andreas Maurer[1,2], Gerald Reischl[1,2], Martin Schaller[3], Irene Gonzalez-Menendez[2,4], Leticia Quintanilla-Martinez[2,4], Meinrad Gawaz[5], Bernd J. Pichler[1,2], Nicolas Beziere[1,6*]

[1]Werner Siemens Imaging Center, Department of Preclinical Imaging and Radiopharmacy, Eberhard Karls University of Tübingen, Germany

[2]Cluster of Excellence EXC 2180 "Image Guided and Functionally Instructed Tumor Therapies" (iFIT), Eberhard Karls University of Tübingen, Germany

[3]Department of Dermatology, University Medical Center, Eberhard Karls University of Tübingen, Germany

[4]Institute of Pathology and Neuropathology, Comprehensive Cancer Center, Eberhard Karls University of Tübingen, Germany

[5]Department of Cardiology and Angiology, University Hospital Tübingen, Eberhard Karls University of Tübingen, Germany

[6]Cluster of Excellence EXC 2124 “Controlling Microbes to Fight Infections” (CMFI), Eberhard Karls University of Tübingen, Germany

Disclaimer: This work has not been published previously, and the manuscript is not under consideration for publication elsewhere. All other authors have declared that no competing interest exists.

*** Corresponding author: Nicolas Beziere**, University of Tübingen, Röntgenweg 13, 72076 Tübingen, Telephone: +49 7071 29-87511, Telefax: +49 7071 29-4451, ORCID: 0000-0002-2076-7060, e-mail: nicolas.beziere@med.uni-tuebingen.de

First author: Simon Isser, University of Tübingen, Röntgenweg 13, 72076 Tübingen, Telephone: +49 7071 29-82975, Telefax: +49 7071 29-4451, e-mail: simon.freisinger@med.uni-tuebingen.de, PhD candidate

Word count: 4902

Running title: PET Imaging of Pulmonary Fibrosis

Financial support: This work was supported by the Werner Siemens Foundation, the *f*ortüne grant (#F1359053) of the Faculty of Medicine of the University of Tübingen and the Deutsche Forschungsgemeinschaft (DFG, German Research Foundation) – Project number 374031971 – TRR 240 (molecular aspects).

ABSTRACT

Invariably fatal and with a particularly fast progression, pulmonary fibrosis (PF) is currently devoid of curative treatment option. Routine clinical diagnosis relies on breathing tests and visualizing the changes in lung structure by computed tomography (CT), but anatomical information is often not sufficient to identify early signs of progressive PF. For more efficient diagnosis, additional imaging techniques were investigated in combination with CT, such as ^{18}F-Fluorodeoxyglucose (^{18}F-FDG) positron emission tomography (PET), although with limited success due to lack of disease specificity. Therefore, novel molecular targets enabling specific diagnosis are investigated, in particular for molecular imaging techniques.

Methods

In this study, we used a ^{64}Cu-radiolabelled platelet glycoprotein VI fusion protein (^{64}Cu-GPVI-Fc), targeting extracellular matrix fibers (ECM) as a PET tracer to observe longitudinally ECM remodeling in a bleomycin-induced PF mouse model.

Results

^{64}Cu-GPVI-Fc showed a significant uptake in fibrotic lungs, matching histology results. Contrary to ^{18}F-FDG PET measurements, ^{64}Cu-GPVI-Fc uptake was entirely linked to the fibrotic activity of tissue and not susceptible to inflammation.

Conclusion

Our study highlights ^{64}Cu-GPVI-Fc as a specific tracer for ECM remodeling in PF, with a clear therapy monitoring and clinical translation potential.

Keywords: pulmonary fibrosis, PET, bleomycin.

Graphical Abstract:

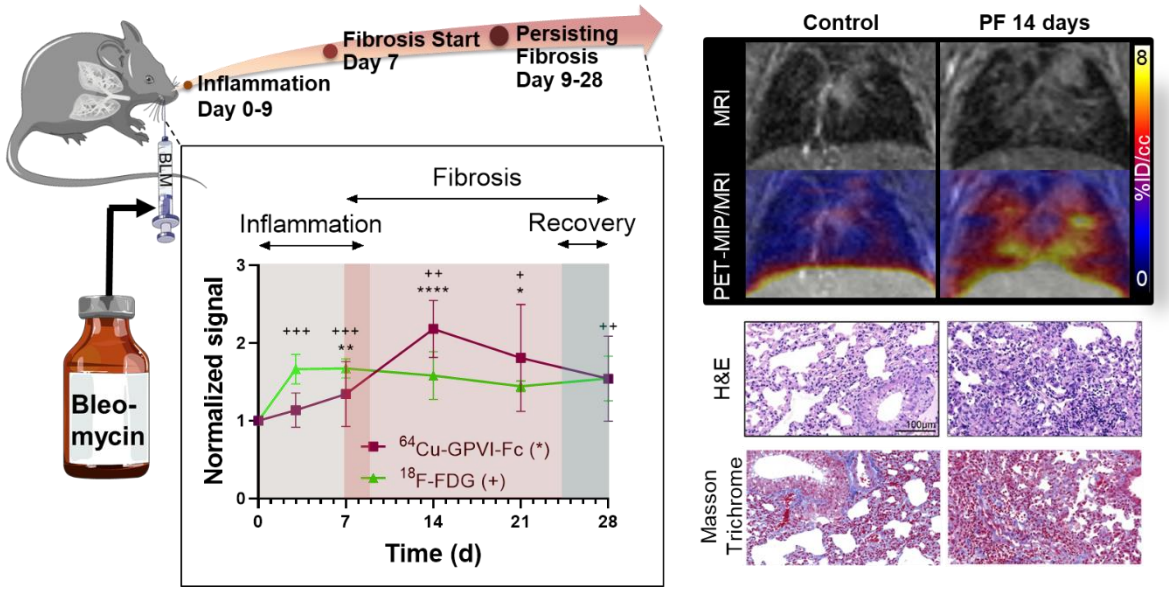
Inflammation
Day 0-9
Fibrosis Start
Day 7
Persisting
Fibrosis
Day 9-28
BLM
Bleo-
mycin
Fibrosis
Inflammation
Recovery
Normalized signal
Time (d)
64Cu-GPVI-Fc (*)
18F-FDG (+)
Control
PF 14 days
MRI
PET-MIP/MRI
%ID/cc
H&E
Masson
Trichrome

1

2

INTRODUCTION

Pulmonary fibrosis (PF) is a fatal disease with a mean life expectancy of 3-5 years after diagnosis (*1*,*2*). It can originate from a myriad of factors such as age or exposure to chemicals and is often rapidly progressing (*3*). Early identification of progressive forms of PF is crucial in populations presenting interstitial lung diseases (ILD) in computed tomography (CT). PF treatment outcome has been shown to be significantly improved following early treatment start (*4*), particularly since the only currently approved drugs against PF (pirfenidone and nintedanib) merely slow down disease progression (*5*). While it is relatively easy to diagnose clinically in its advanced stage despite unspecific symptoms due to the characteristic lung honeycombing visible in CT, early stages of progressive-fibrosing ILD remain very difficult to identify (*6*). High-resolution CT (HRCT) can provide increased sensitivity and better recognition of abnormalities in potential PF patients than regular CT, justifying its current central role in PF diagnosis (*7*,*8*), but early screening of ILD populations cannot rely on HRCT alone as it only provides a snapshot of anatomical structures. Accessing early biomarkers of the disease, ideally by imaging methods, could enable early screening of patients at risk of progressive-fibrosing ILD, monitoring of disease progression and provide a novel way to assess treatment efficacy. ^{18}F-FDG PET imaging has shown moderate success in PF patients (*9*-*11*), as this radiotracer only reflects glucose uptake and cannot distinguish between inflammation, fibrosis and malignant cell proliferation and can thus provide misleading results.

Remodeling of tissue in PF occurs through the increased deposition of extracellular matrix (ECM) fibers such as collagen I-III, fibronectin and fibrinogen, which marks the disease onset and early progression. As such, these fibers represent ideal biomarkers for early PF diagnosis, and radiotracers targeting individual fibers such as collagen I have been developed and have

shown promising results preclinically and clinically (*12*). However, there are currently no radiotracers able to provide an overall picture of ECM remodeling during progressive PF. Interestingly, nature provides a molecule able to targets several ECM fibers, e.g. collagen I-III, fibronectin and fibrinogen (*13-15*), platelet glycoprotein VI (GPVI). GPVI is naturally expressed on the surface of platelets and megakaryocytes and plays a crucial role in their aggregation during wound repair due to its high affinity after dimerization for the aforementioned ECM fibers (*16,17*). To capitalize on this high affinity, an IgG1 GPVI fusion protein (GPVI-Fc) mimicking highly affine GPVI dimers has been previously synthesized and initially investigated as an antithrombotic agent (*18*). Imaging using fluorescent GPVI-Fc and a ^{64}Cu radiolabeled GPVI-Fc ^{64}Cu-NOTA-GPVI-Fc (^{64}Cu-GPVI-Fc) could show the potential of this targeting vector in thrombosis imaging (*19,20*) as well as in several models presenting a fibrotic component such as rheumatoid arthritis and cutaneous delayed-type hypersensitivity reaction (*21*). While some of these diseases are predominantly of an inflammatory nature, with fibrosis appearing at a later stage, tracer uptake could be correlated with changes in the ECM and shown in *in vivo* imaging experiments and *ex vivo* histology.

Here, we investigate the potential of ^{64}Cu-GPVI-Fc for early detection of PF and monitoring of its progression in the bleomycin-induced PF mouse model. Our objective was the visualization and quantification of progressive PF longitudinally, non-invasively and with high disease specificity and the potential of the approach in comparison to ^{18}F-fluorodeoxyglucose (^{18}F-FDG) PET imaging of PF.

MATERIALS AND METHODS

The full version of the Materials and Methods can be found in Supplemental Material. Figure 1 shows the study workflow.

Radiotracer Synthesis

^{18}F-FDG was produced using a TRACERlab MX module (GE Healthcare, Liège, Belgium) with radiochemical purity over 95%. ^{64}Cu-GPVI-Fc was produced as described previously with a radiochemical purity of over 95% (*21*). To perform isotype experiments, NOTA-GPVI-Fc was denatured according to the procedure developed by Akazawa-Ogawa *et al.* (*22*) by incubation for 30 min at 70°C and subsequently radiolabelled using the same procedure as with stock NOTA-GPVI-Fc with a radiochemical purity of over 70%. Denatured ^{64}Cu-GPVI-Fc is referred to herein as radiolabeled isotype.

Pulmonary Fibrosis Model

Animal experiments were performed in accordance to the German Animal Protection Law protocols for animal use and care, approved by the Regierungspräsidium Tübingen (NTP-ID: 00034862-5-7). In short, 1 mg/kg body weight of bleomycin in 50 µL saline was deposited intra-tracheally in 8 weeks old C57BL/6J female mice (50 µL saline only in control animals) at day 0, following the procedure described by Walters *et al.* (*23*). For ethical reasons, animals presenting a weight loss of over 20% or showing significant signs of suffering were sacrificed and not included in the study. Group size for each experiment can be found in Supplemental Material.

Positron Emission Tomography and Magnetic Resonance Imaging

High resolution PET scans were performed using Inveon small-animal PET scanners (Siemens Healthcare, Erlangen, Germany) with Inveon Acquisition Workplace Version 2.1.272 Software (Siemens Medical Solutions, Knoxville TN 37932, USA). Tracers (one per animal group) were injected in the tail vein (12±1.2 MBq): ^{18}F-FDG was injected 5 s after the start of a 1 h dynamic

scan followed by an 827 s transmission scan; ^{64}Cu-GPVI-Fc was imaged with a 10 min static scan 3 h, 24 h and 48 h post injection (p.i.). Each PET scan was followed by magnetic resonance imaging (MRI) sequences for anatomical reference using a 7-T small-animal scanner (ClinScan; Bruker Biospin MRI GmbH, Ettlingen, Germany) with the Paravision 6.0.1 Software (Bruker Corporation, Billerica MA 01821, USA). PET images were coregistered with MRI images using fiducial markers and analyzed with Inveon Research Workplace software (Siemens Healthcare) by drawing regions of interest on the MRI image and applying them onto the PET images for volumetric quantification of radiotracer accumulation in the entire lung for ^{64}Cu radiotracer injected animals and in the right lung lobes for ^{18}F-FDG injected animals.

Biodistribution

Mice were sacrificed using CO_2, perfused with 20 mL 4°C phosphate buffered saline (PBS) through the right ventricle and organ samples were explanted for activity measurements *ex vivo* using a 2480 Automatic Gamma Counter WIZARD$^{2®}$ from PerkinElmer (Waltham, Massachusetts, USA).

Histology

For hematoxylin and eosin (H&E) and Masson trichrome (MT) staining, perfused lungs were fixated in formalin, embedded in paraffin and then cut in 5 µm thick slices using a microtome (Leica, Wetzlar, Germany). All samples were scanned with the Nanozoomer (Hamamatsu) and processed with the programs Case Viewer. Photomicrographic images were acquired with an Axioskop 2 plus Zeiss microscope equipped with a Jenoptik (Laser Optik System, Jena, Germany) ProgRes C10 plus camera and software. Final image preparation was performed with Adobe Photoshop CS6. Scoring of inflammation was performed based on H&E as follows: 0 (no inflammation), 1 (mild inflammation), 2 (moderate inflammation) and 3 (prominent inflammation). Fibrosis scoring was done following the modified Ashcroft scale (*24*).

For fluorescence microscopy, frozen lung slices were labeled with anti-fibronectin, anti-fibrinogen, anti-collagen I, anti-collagen II or anti-collagen III primary antibodies. For secondary antibody anti-rabbit Cy3 was used to visualize ECM fibers and anti-human IgG-Cy5 was used to visualize NOTA-GPVI-Fc. Nuclei were stained using YO-PRO-1 and images were acquired using a Zeiss LSM 800 system (Carl Zeiss, Oberkochen, Germany) with ZEN 2.3 (blue edition) software.

Data Evaluation and Statistics

Statistical analysis was performed using Ordinary one-way ANOVA (Multiple comparison test based on Dunnett's correction) in GraphPad Prism 9.0.1 for comparison of lungs at different time points, groups were compared to respective control. For *ex vivo* biodistribution comparison of different organs mixed-effects analysis was used, groups were compared to respective control. For comparison between uptake of ^{64}Cu-GPVI-Fc and radiolabeled isotype control unpaired t-test was used. For histological scoring evaluation two-way ANOVA was used. Significant results are depicted using * ($P \leq 0.05$), ** ($P \leq 0.01$), *** ($P \leq 0.001$) and **** ($P \leq 0.0001$). Results show each individual data point together with the mean of each group and its standard deviation. γ-counter results from one mouse in the ^{18}F-FDG study was identified as outlier by Grubb's test, originating from a user error during *ex vivo* uptake measurement, and removed from further statistical *ex vivo* evaluation.

RESULTS

^{64}Cu-GPVI-Fc Imaging of Pulmonary Fibrosis Progression in a C57Bl/6J Bleomycin Model

Imaging measurements were performed 3, 7, 14, 21, 28 days post deposition (p.d.) of bleomycin (Figure 1). ^{64}Cu-GPVI-Fc distribution was quantified during PF progression after MRI-guided organ segmentation to investigate ECM remodeling in bleomycin exposed C57BL/6J. Preliminary experiments performed 3, 24 and 48h after injection of ^{64}Cu-GPVI-Fc indicated the optimal uptake ratio in diseased animals could be attained 48h after tracer injection (Supplemental Figure 1). Pulmonary uptake of ^{64}Cu-GPVI-Fc 48h after injection was visibly increased *in vivo* 7, 14 and 21 days p.d. compared to control (Figure 2A). Quantification of *in vivo* measurements (Figure 2B) showed no significant difference in radiotracer accumulation 3 days p.d. compared to control. Afterwards, lung uptake was significantly higher compared to control from 7 days p.d., peaking at 14 days with a contrast ratio of 1.74, till 21 days p.d. (3.54±0.26 %ID/cc, 4.32±0.60 %ID/cc and 3.41±1.06 %ID/cc respectively). 28 days p.d., no significantly increased uptake compared to control was observed. *Ex vivo* measurement of ^{64}Cu-GPVI-Fc accumulation in the lungs confirmed a significant higher uptake 14 days p.d. and 21 days p.d. compared to control (7.44±1.26 %ID/g, 6.17±2.35 %ID/g and 3.41±0.75 %ID/g, $P \leq 0.0001$ and $P \leq 0.01$ respectively) (Figure 2C). Analysis of *ex vivo* tracer biodistribution showed limited changes in other organs (Supplemental Figure 2) with only the blood pool signal being lower 28 days p.d. compared to control (2.45±0.59 %ID/g to 2.91±0.41 %ID/g, $P \leq 0.05$). Pathological changes were clearly visible in H&E and MT histology sections (Figure 3A). Mild and focal inflammatory infiltrates were seen day 3 p.d., followed by more intense inflammatory infiltrates and minimal fibrosis day 7. Fibrosis reached its peak on 14 days p.d., followed by a small reduction in fibrotic areas at 21 days and 28 days p.d. (Supplemental Figure 3). Scoring

(Figure 3B) highlighted a significant increase in inflammation day 7 p.d. (2.00±0) and day 14 p.d. (2.00±0), followed by a decline at day 21 p.d. (1.00±0). Day 3 and 28 p.d. did not display a significant increase in immune cell infiltration compared to control. Modified Ashcroft scoring obtained from entire lung sections, composed of both healthy parenchyma and fibrotic areas, was higher than control at day 7 p.d. (1.27±0.28), but reached its peak on day 14 p.d. (2.72±0.44) and day 21 p.d. (1.96±0.42). Day 28 p.d. presented a minor increase in fibrosis compared to control (1.29±0.9). Fluorescence microscopy showed co-localization of GPVI-Fc and ECM fibers, such as collagen I, II, III, fibronectin and fibrinogen 14 days p.d., with collagen III and fibronectin showing extensive co-localization. (Figure 3C).

Specificity of ^{64}Cu-GPVI-Fc for Fibrosis

To further investigate ^{64}Cu-GPVI-Fc specificity towards fibrosis in mouse lungs after bleomycin deposition, we performed binding experiments using a heat-denatured ^{64}Cu-radiolabelled GPVI-Fc (isotype). A lower uptake of the isotype was visible 14 days p.d. compared to intact ^{64}Cu-GPVI-Fc (Figure 4A) 48 h post tracer injection (2.46±0.56 %ID/cc to 4.32±0.60 %ID/cc, $P < 0.0001$) (Figure 4B), confirmed by *ex vivo* measurement (4.37±0.48 %ID/g and 7.44±1.26 %ID/g %ID/g, $P \leq 0.0001$) (Figure 4C). The radiolabeled isotype showed accumulation in diseased animals close to the accumulation of ^{64}Cu-GPVI-Fc in control animals. *Ex vivo* biodistribution (Supplemental Figure 4) showed a significantly lower uptake in all measured organs compared to intact ^{64}Cu-GPVI-Fc, except in the spleen with a significantly higher uptake of the radiolabeled isotype compared to intact ^{64}Cu-GPVI-Fc (16.55±3.93 %ID/g and 9.02±2.43 %ID/g, $P \leq 0.05$).

^{18}F-FDG Imaging of Pulmonary Fibrosis in Bleomycin Inoculated C57Bl/6J Mice

To visualize glucose metabolism during progression of PF, we used ^{18}F-FDG-PET in a distinct set of animals as it is considered the reference radiotracer even in PF imaging research (*25*) (Figure 5A). Quantification of radiotracer accumulation *in vivo* (Figure 5B), showed a significantly increased uptake at all time-points, remaining stable throughout the course of the experiment (4.70±0.56 %ID/cc in control and 7.77±0.92 %ID/cc day 3, 7.82±1.14 %ID/cc day 7, 7.39±1.45 %ID/cc day 14, 6.74±0.41 %ID/cc day 21 and 7.21±1.46 %ID/cc day 28, with $P \leq 0.001$, $P \leq 0.001$, $P \leq 0.01$, $P \leq 0.05$ and $P \leq 0.01$,). This behavior was also seen *ex vivo* (Figure 5C) at day 3, 7, 14 and 21 p.d. (4.65±0.58 %ID/g, 14.10±3.74 %ID/g, 12.17±1.49 %ID/g, 12.20±3.52 %ID/g and 13.70±2.92 %ID/g, with $P \leq 0.01$, $P \leq 0.05$, $P \leq 0.05$ and $P \leq 0.01$), but not day 28 (10.30±3.91 %ID/g). Complete biodistribution analysis however showed no difference in uptake in other organs (Supplemental Figure 5). Blood glucose measurements showed that blood glucose levels had no influence on ^{18}F-FDG uptake in this experiment (Supplemental Table 1).

DISCUSSION

In this study, we used PET imaging of the ECM fibers targeting radiotracer ^{64}Cu-GPVI-Fc to monitor fibrosis progression in a bleomycin murine model of PF, and investigated its potential for early and specific diagnosis of the disease. We could show that the significantly increased pulmonary uptake of ^{64}Cu-GPVI-Fc found at 14 and 21 days p.d. aligned with both *ex vivo* biodistribution analysis and histological validation, with Ashcroft scoring highlighting acute fibrosis during the second and third week of disease progression. These findings are in line with the reported PF progression in this model, with a second and third week peak fibrotic activity (*23,26,27*). 7 days p.d. however, a small increase in ^{64}Cu-GPVI-Fc accumulation could be seen *in vivo* but not confirmed *ex vivo*: to dismiss the possibility of inflammation driven ^{64}Cu-GPVI-Fc accumulation in bleomycin deposited animals, as the bleomycin model shows early inflammation during the first two weeks in contrary to the human presentation of the disease (*23,26,27*), we performed radiolabeled isotype experiments using heat denatured GPVI-Fc. No specific lung accumulation of the isotype radiotracer could be seen *in vivo* 14 days p.d., a time point presenting both fibrosis and inflammation. While a signal coming from the heart could be seen in control and diseased animals using ^{64}Cu-GPVI-Fc, the isotype showed a reduction in heart signal, likely due to the overall reduced circulation time of the radiotracer due to the denaturation of the Fc fragment of the protein. In addition, fluorescence microscopy highlighted co-localization of NOTA-GPVI-Fc with different ECM fibers, such as collagen I-III, fibronectin and fibrinogen. Interestingly, radiotracer accumulation was reduced 28 days p.d., as was MT staining. This corresponds to the so-called resolution phase of the disease, characteristic of the bleomycin animal model (*28*). Taken together, these findings underline the specific binding potential of the tracer during progressive fibrosis and its accuracy to detect early PF progression *in vivo*.

As a reference point, ^{18}F-FDG experiments were performed *in vivo* following the same experimental plan. The increase in ^{18}F-FDG PET uptake at all-time points p.d., covering inflammatory and fibrotic stages in the mouse model, highlights the poor specificity of ^{18}F-FDG for PF as this radiotracer merely reports glucose uptake regardless of its origin, including the inflammatory phase present during the first week of the bleomycin murine model. This showcases ^{64}Cu-GPVI-Fc potential for early and specific detection of progressive fibrosis. Achieving a good correlation between ^{18}F-FDG-PET imaging and positive PF diagnosis requires complex, expensive and time consuming measurements, impractical in clinical routine (*10*), which could be avoided by the use of a specific radiotracer. Furthermore, changes in ^{18}F-FDG uptake were not detectable in a clinical study three-month post pirfenidone treatment (*29*). This significantly limits the use of ^{18}F-FDG in the clinics for early PF diagnosis and therapy monitoring and underlines the necessity for specific non-invasive detection of progressive PF.

Different tracers targeting ECM changes have been reported (*30*). In particular, collagen I targeting PET showed a behavior similar to ^{64}Cu-GPVI-Fc with similar results over time *in vivo* in mice (*12*). In addition, this collagen I tracer was used in rats (*31*), with comparable results to our study albeit with a shifted timeline likely due to the difference in model species. ^{68}Ga-pentixafor, targeting CXCR4, a protein upregulated in cancer as well as during progressive PF, has shown promising results in clinical trials, including a correlation between evolution of uptake and pirfenidone treatment outcome (*32*). Significant work on the fibroblast activation protein (FAP) highlighted its involvement in the progression of PF and sprouted the use of FAP targeted radiotracers for PF imaging (*33*), which are also leading to promising results in the clinic (*34*). In contrast, ^{64}Cu-GPVI-Fc targets multiple collagen subtypes (I, II, III) as well as fibronectin and fibrinogen (*13-15*), which are found in lung fibrotic regions with high amount of myofibroblasts, and are known to synergize to drive the ECM remodeling (*35*). Thus, ^{64}Cu-GPVI-Fc may provide

an alternative, more complete view of disease progression, possibly allowing for earlier detection of progressive forms of pulmonary fibrosis.

CONCLUSION

Here, we showed that ^{64}Cu-GPVI-Fc displays specific uptake during the progressive stage of PF in the bleomycin mouse model, but not during the initial inflammatory phase specific to the bleomycin model. This specific uptake was confirmed *ex vivo* and provides a new approach by targeting multiple ECM components, giving access to a broad picture of PF progression. Therefore, ^{64}Cu-GPVI-Fc represents a new tool to image PF progression *in vivo*, with high clinical translation potential, able to distinguish between progressive fibrosis and inflammation effectively.

DISCLOSURE

All authors have declared that no competing interest exists. This work was supported by the Werner Siemens Foundation, by the *f*ortüne grant (#F1359053) of the Faculty of Medicine of the University of Tübingen and the Deutsche Forschungsgemeinschaft (DFG, German Research Foundation) – Project number 374031971 – TRR 240 (molecular aspects).

ACKNOWLEDGMENTS

We thank Linda Schramm, Miriam Owczorz, Walter Ehrlichmann, Dominik Seyfried and Johannes Kinzler for their technical support, as well as Götz Münch from advanceCOR GmbH (82152 Planegg, Germany) for supplying GPVI-Fc. The Graphical Abstract and Figure1 were partly generated using Servier Medical Art, provided by Servier, licensed under a Creative Commons Attribution 3.0 unported license.

KEY POINTS

Question: Can ECM disruption be used as an early marker to depict progressive pulmonary fibrosis in a pre-clinical mouse model using ^{64}Cu-GPVI-Fc PET imaging?

Pertinent Findings: A preclinical bleomycin induced pulmonary fibrosis mouse model was studied longitudinally using PET imaging of ^{64}Cu-GPVI-Fc. The radiotracer showed high specificity towards the fibrotic phase of the disease model *in vivo*, as shown by histology and fluorescence microscopy *ex vivo.*

Implications for Patient Care: ^{64}Cu-GPVI-Fc PET imaging could help in early stratification of patients presenting ILD in classical HRCT and identifying of early signs of progressive fibrosis the necessity of an invasive biopsy and therefore lead to an earlier treatment start.

REFERENCES

1. King TE, Pardo A, Selman M. Idiopathic pulmonary fibrosis. *The Lancet.* 2011;378:1949-1961.

2. Chen X, Guo J, Yu D, Jie B, Zhou Y. Predictors of mortality in progressive fibrosing interstitial lung diseases. *Front Pharmacol.* 2021;12:754851.

3. Raghu G. Idiopathic pulmonary fibrosis: lessons from clinical trials over the past 25 years. *Eur Respir J.* 2017;50.

4. Antoniou KM, Symvoulakis EK, Margaritopoulos GA, Lionis C, Wells AU. Early diagnosis of IPF: time for a primary-care case-finding initiative? *Lancet Respir Med.* 2014;2:e1.

5. Finnerty JP, Ponnuswamy A, Dutta P, Abdelaziz A, Kamil H. Efficacy of antifibrotic drugs, nintedanib and pirfenidone, in treatment of progressive pulmonary fibrosis in both idiopathic pulmonary fibrosis (IPF) and non-IPF: a systematic review and meta-analysis. *BMC Pulm Med.* 2021;21:411.

6. Cottin V, Hirani NA, Hotchkin DL, et al. Presentation, diagnosis and clinical course of the spectrum of progressive-fibrosing interstitial lung diseases. *Eur Respir Rev.* 2018;27:180076.

7. Walsh SLF, Devaraj A, Enghelmayer JI, et al. Role of imaging in progressive-fibrosing interstitial lung diseases. *Eur Respir Rev.* 2018;27:180073.

8. Abu Qubo A, Capaccione KM, Bernstein EJ, Padilla M, Salvatore M. The role of radiology in progressive fibrosing interstitial lung disease. *Front Med (Lausanne).* 2021;8:679051.

9. Castiaux A, Van Simaeys G, Goldman S, Bondue B. Assessment of 18F-FDG uptake in idiopathic pulmonary fibrosis: influence of lung density changes. *Eur J Hybrid Imaging.* 2018;2:27.

10. Fraioli F, Lyasheva M, Porter JC, et al. Synergistic application of pulmonary 18 F-FDG PET/HRCT and computer-based CT analysis with conventional severity measures to refine current risk stratification in idiopathic pulmonary fibrosis (IPF). *Eur J Nucl Med Mol Imaging.* 2019;46:2023-2031.

11. Ko UW, Yoon H-y, Lee SH, et al. The Value of 18F-FDG PET/CT in evaluating disease severity in idiopathic pulmonary fibrosis. *Eur Respir J.* 2017;50:PA850.

12. Désogère P, Tapias LF, Hariri LP, et al. Type I collagen–targeted PET probe for pulmonary fibrosis detection and staging in preclinical models. *Sci Transl Med.* 2017;9:eaaf4696.

13. Moroi M, Jung SM. Platelet glycoprotein VI: its structure and function. *Thromb Res.* 2004;114:221-233.

14. Induruwa I, Moroi M, Bonna A, et al. Platelet collagen receptor Glycoprotein VI-dimer recognizes fibrinogen and fibrin through their D-domains, contributing to platelet adhesion and activation during thrombus formation. *J Thromb Haemost.* 2018;16:389-404.

15. Mangin PH, Onselaer MB, Receveur N, et al. Immobilized fibrinogen activates human platelets through glycoprotein VI. *Haematologica.* 2018;103:898-907.

16. Chen H, Locke D, Liu Y, Liu C, Kahn ML. The platelet receptor GPVI mediates both adhesion and signaling responses to collagen in a receptor density-dependent fashion. *J Biol Chem.* 2002;277:3011-3019.

17. Jung SM, Moroi M. Platelet glycoprotein VI. *Adv Exp Med Biol.* 2008;640:53-63.

18. Ungerer M, Rosport K, Bultmann A, et al. Novel antiplatelet drug revacept (Dimeric Glycoprotein VI-Fc) specifically and efficiently inhibited collagen-induced platelet aggregation without affecting general hemostasis in humans. *Circulation.* 2011;123:1891-1899.

19. Bigalke B, Lindemann S, Schonberger T, et al. Ex vivoimaging of injured arteries in rabbits using fluorescence-labelled glycoprotein VI-Fc. *Platelets.* 2012;23:1-6.

20. Bigalke B, Phinikaridou A, Andia ME, et al. Positron emission tomography/computed tomographic and magnetic resonance imaging in a murine model of progressive atherosclerosis using (64)Cu-labeled glycoprotein VI-Fc. *Circ Cardiovasc Imaging.* 2013;6:957-964.

21. Beziere N, Fuchs K, Maurer A, et al. Imaging fibrosis in inflammatory diseases: targeting the exposed extracellular matrix. *Theranostics.* 2019;9:2868-2881.

22. Akazawa-Ogawa Y, Nagai H, Hagihara Y. Heat denaturation of the antibody, a multi-domain protein. *Biophys Rev.* 2018;10:255-258.

23. Walters DM, Kleeberger SR. Mouse models of bleomycin-induced pulmonary fibrosis. *Curr Protoc Pharmacol.* 2008;Chapter 5:Unit 5 46.

24. Hubner RH, Gitter W, El Mokhtari NE, et al. Standardized quantification of pulmonary fibrosis in histological samples. *Biotechniques.* 2008;44:507-511, 514-507.

25. Mahmutovic Persson I, von Wachenfeldt K, Waterton JC, Olsson LE, Medicine TCJJoC. Imaging biomarkers in animal models of drug-induced lung injury: a systematic review. *J Clin Med.* 2021;10:107.

26. Mouratis MA, Aidinis V. Modeling pulmonary fibrosis with bleomycin. *Curr Opin Pulm Med.* 2011;17:355-361.

27. Moore BB, Hogaboam CM. Murine models of pulmonary fibrosis. *Am J Physiol Lung Cell Mol Physiol.* 2008;294:L152-160.

28. Tashiro J, Rubio GA, Limper AH, et al. Exploring animal models that resemble idiopathic pulmonary fibrosis. *Front Med (Lausanne).* 2017;4:118.

29. Bondue B, Castiaux A, Van Simaeys G, et al. Absence of early metabolic response assessed by 18F-FDG PET/CT after initiation of antifibrotic drugs in IPF patients. *Respir Res.* 2019;20:10.

30. Désogère P, Montesi SB, Caravan PJCAEJ. Molecular probes for imaging fibrosis and fibrogenesis. *Chem Eur J.* 2019;25:1128-1141.

31. Mahmutovic Persson I, Fransén Pettersson N, Liu J, et al. Longitudinal imaging using PET/CT with Collagen-I PET-tracer and MRI for assessment of fibrotic and inflammatory lesions in a rat lung injury model. *J Clin Med.* 2020;9:3706.

32. Derlin T, Jaeger B, Jonigk D, et al. Clinical molecular imaging of pulmonary CXCR4 expression to predict outcome of pirfenidone treatment in idiopathic pulmonary fibrosis. *Chest.* 2021;159:1094-1106.

33. Lindner T, Loktev A, Altmann A, et al. Development of quinoline-based theranostic ligands for the targeting of fibroblast activation protein. *J Nucl Med.* 2018;59:1415-1422.

34. Röhrich M, Leitz D, Glatting FM, et al. Fibroblast activation protein–specific PET/CT imaging in fibrotic interstitial lung diseases and lung cancer: a translational exploratory study. *J Nucl Med.* 2022;63:127-133.

35. Herrera J, Henke CA, Bitterman PB. Extracellular matrix as a driver of progressive fibrosis. *J Clin Invest.* 2018;128:45-53.

Figures

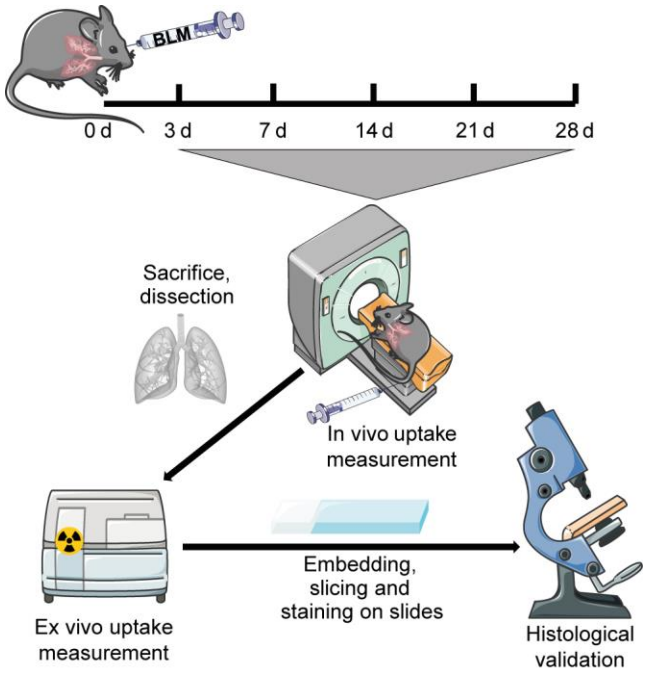

Figure 1: Experimental workflow for longitudinal pulmonary fibrosis imaging. Day 0: intra tracheal deposition of bleomycin (BLM) or saline. Day 3, 7, 14, 21 or 28 post bleomycin deposition: positron emission tomography (PET) and magnetic resonance imaging (MRI) scans after radiotracer injection. Post *in vivo* imaging: sacrifice, biodistribution, microscopy imaging.

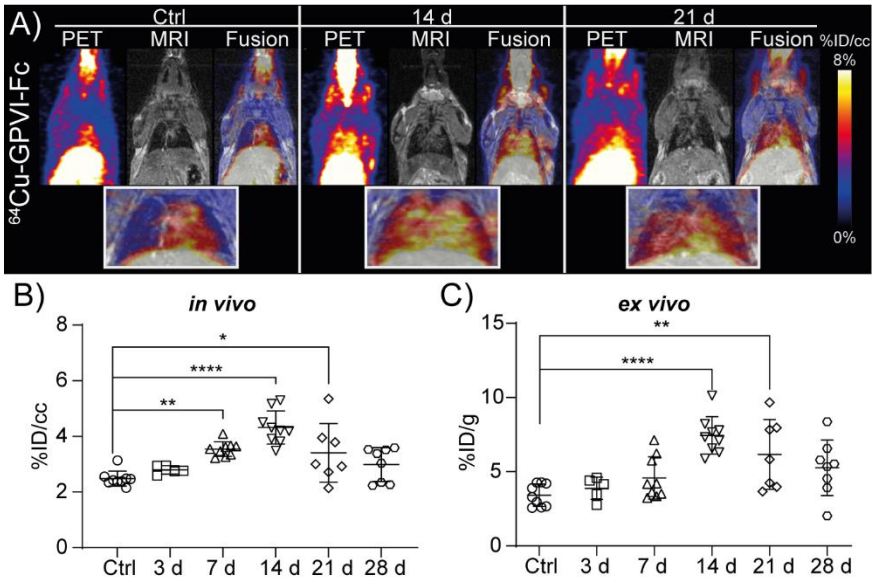

Figure 2: Imaging of bleomycin induced pulmonary fibrosis C57BL/6J mouse model using ^{64}Cu-NOTA-GPVI-Fc. (^{64}Cu-GPVI-Fc). (A) Representative images of ^{64}Cu-GPVI-Fc accumulation 48 h after radiotracer injection acquired in animals deposited intra-tracheally with saline (Ctrl) or bleomycin 14 or 21 days post deposition (14 d or 21 d). Maximum intensity projection PET images co-localized with single slice MRI (fusion) (n: 4-9). (B) Corresponding quantification of *in vivo* tracer uptake in percentage injected dose per cubic centimeter [%ID/cc] in the lung in control animals (Ctrl) or at various days after bleomycin deposition. (C) Corresponding quantification of *ex vivo* tracer uptake [%ID/g] in the lungs. * ($P \leq 0.05$), ** ($P \leq 0.01$), *** ($P \leq 0.001$) and **** ($P \leq 0.0001$).

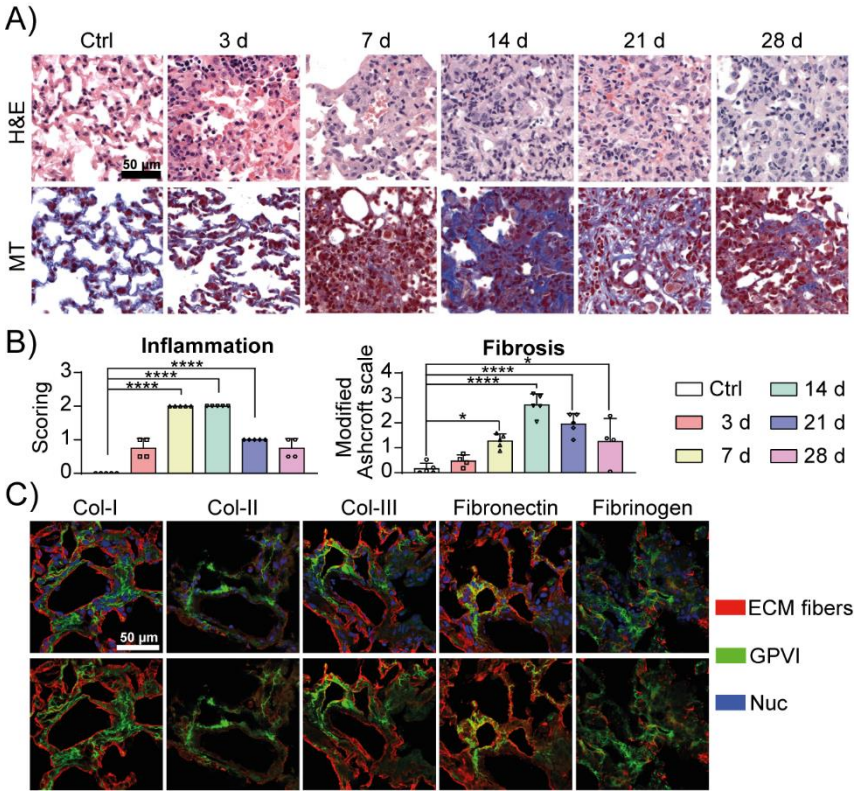

Figure 3: Ex vivo microscopic imaging of bleomycin induced pulmonary fibrosis C57BL/6J mouse lungs. (A) Hematoxylin & Eosin (H&E) and Masson trichrome (MT) stains of control animals and at day 3, 7, 14, 21 and 28 post bleomycin deposition. Scale in control H&E image depicts 50 µm, MT images are depicted at the same scale. (B) Histology scoring of inflammation and modified Ashcroft score (n: 4-5) in mouse lungs at all time-points compared to control. (C) Fluorescence microscopy for co-localization of GPVI-Fc (shown in green) with the extra cellular matrix (ECM) fibers (red) Collagen I-III (Col-I-III), Fibronectin and Fibrinogen, nuclei (Nuc, blue) to localize cells. Scale in Col-I image depicts 50 µm. * ($P \leq 0.05$), ** ($P \leq 0.01$), *** ($P \leq 0.001$) and **** ($P \leq 0.0001$).

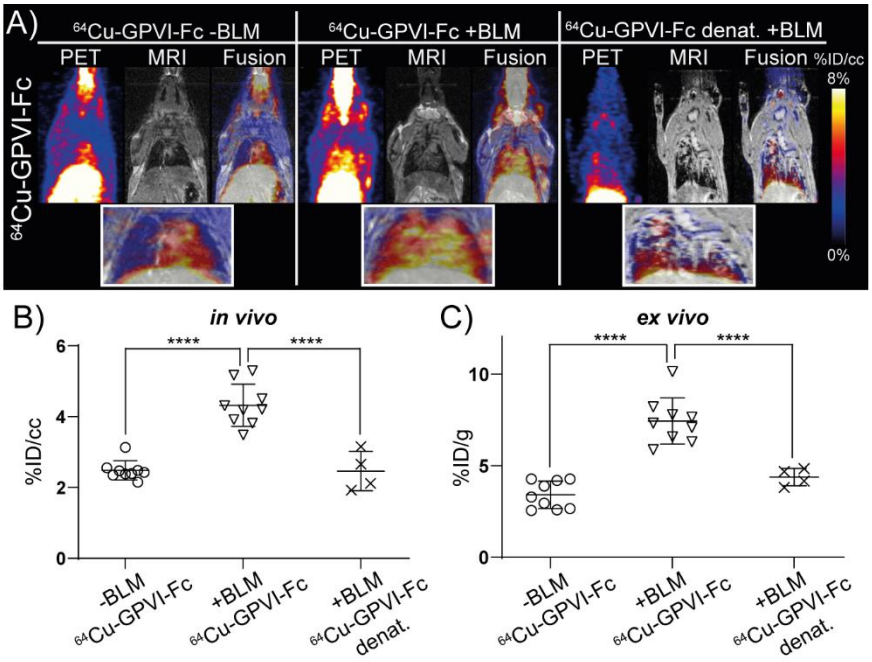

Figure 4: Uptake specificity of ^{64}Cu-NOTA-GPVI-Fc (^{64}Cu-GPVI-Fc). (A) Representative images of maximum intensity projection PET images of control (^{64}Cu-GPVI-Fc -BLM, left, n=9) and bleomycin (BLM)-induced fibrotic animals injected with ^{64}Cu-GPVI-Fc (^{64}Cu-GPVI-Fc +BLM, middle, n=9) and fibrotic animals injected with denatured ^{64}Cu-GPVI-Fc (^{64}Cu-GPVI-Fc denat. +BLM, right, n=4) 14 days post bleomycin deposition co-localized with single slice MRI (fusion). (B) Corresponding *in vivo* quantification in the lungs in percentage injected dose per cubic centimeter [%ID/cc]. (C) Corresponding *ex vivo* quantification of tracer uptake [%ID/g] in the lungs.* ($P \leq 0.05$), ** ($P \leq 0.01$), *** ($P \leq 0.001$) and **** ($P \leq 0.0001$).

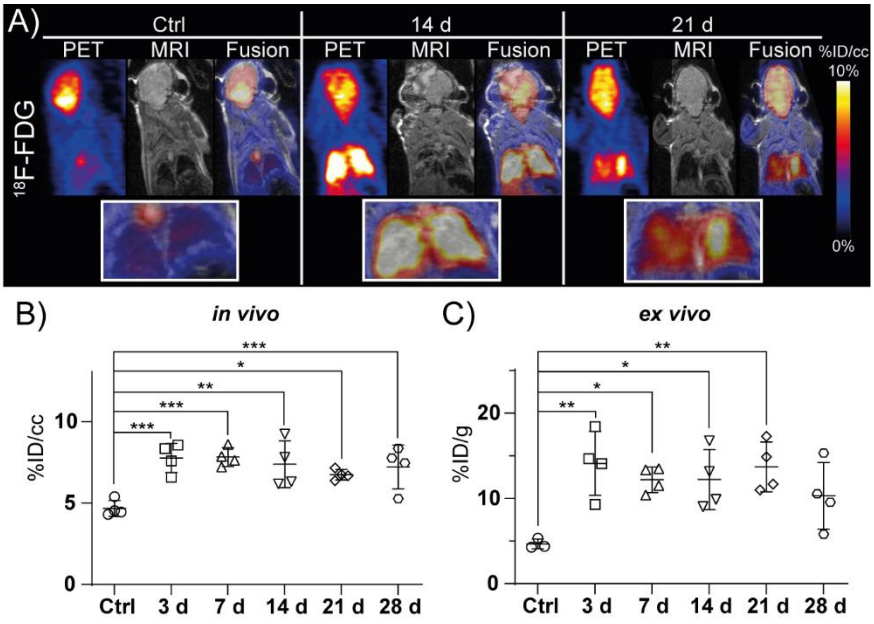

Figure 5: ^{18}F-FDG-PET imaging of C57Bl/6J mice with bleomycin induced pulmonary fibrosis. (A) Representative images of single slice PET images co-localized with single slice MRI (fusion) 14 and 21 days post bleomycin (BLM) deposition (14 d and 21 d) and in control (Ctrl) (n=4-5). (B) Evaluation of mean *in vivo* tracer uptake from 2-60 min post tracer injection in percentage injected dose per cubic centimetre [%ID/cc]. (C) Evaluation of *ex vivo* tracer uptake in percentage injected dose per gram [%ID/g] in the same lungs. (E) Mean dynamic *in vivo* uptake normalized to injected dose per cubic centimetre [%ID/cc] in the right lung lobes over one hour for control, 3 days, 7 days, 14 days, 21 days and 28 days post deposition. Red: time interval used to calculate the mean uptake in each mouse. * ($P \leq 0.05$), ** ($P \leq 0.01$) and *** ($P \leq 0.001$).

Supplemental Material to:

Radiolabeled GPVI-Fc for PET imaging of multiple extracellular matrix fibers: A new look into pulmonary fibrosis progression.

MATERIALS AND METHODS

Radiotracer Synthesis

^{18}F-fluorodeoxyglucose (^{18}F-FDG) was produced using a TRACERlab MX module (GE Healthcare, Liège, Belgium) as for clinical application (radiochemical purity: HPLC and TLC≥95%). ^{64}Cu -NOTA-GPVI-Fc (^{64}Cu-GPVI-Fc) was produced as described previously (*1*). In short, GPVI-Fc (Revacept ®) was provided by advanceCOR (Munich, Germany) and conjugated with p-SCN-Bn-NOTA (2-S-(4-isothiocyanatobenzyl)-1,4,7-triazacyclononane-1,4,7-triacetic acid, Macrocyclics, Plano, TX, USA), radiolabelled with ^{64}Cu-Cl_2 (produced in-house at the GE PETtrace cyclotron (GE, Uppsala, Sweden) in a ratio of 2 µg/MBq and analyzed for purity and appearance, identity, chemical and radiochemical purity (HPLC and TLC≥95% for naïve tracer, TLC≥70% for denatured tracer control), pH, radionuclidic purity (gamma-spectrometry), endotoxins, and sterility. To perform isotype experiments, NOTA-GPVI-Fc was denatured according to the procedure developed by Akazawa-Ogawa *et al.* (*2*) for loss of specific binding activity of IgG antibodies. In short, the NOTA-GPVI-Fc was heated up to 70°C, followed by incubation for 30min at 70°C. Afterwards, the denatured NOTA-GPVI-Fc was cooled down to RT and stored in a fridge until radiolabelling; using the same procedure as with stock NOTA-GPVI-Fc. Denatured ^{64}Cu-GPVI-Fc is referred to as radiolabeled isotype in this study.

Pulmonary Fibrosis Model

Animal experiments were performed in accordance to the German Animal Protection Law protocols for animal use and care, approved by the Regierungspräsidium Tübingen (NTP-ID: 00034862-5-7). Female C57BL/6J or Balb/c mice were purchased from Charles River Laboratory at the age of 7-9 weeks, and were given one week to acclimate to our animal facility. Mice were then anesthetized by intra peritoneal (i.p.) injection of 80 mg/kg ketamine and 15 mg/kg xylazine. The BLM solution was prepared with a concentration of 0.5 mg/mL and a single dose of BLM (1 mg/kg body weight) was deposited intra-tracheally in 50 µL of saline per mouse. The control group received 50 µL saline. Intra tracheal deposition was performed following Walters *et al.* (*3*). In brief, after reaching deep anesthesia mice were fixated on their back on an approximately 60° tilted board with face up. A tube was inserted into the trachea and the BLM solution or pure saline was deposited into the tube, immediately followed by ventilation by air (frequency: 250 per minute, volume: 300 µL, duration: 30 s) to ensure equal distribution of the solution. For the ^{18}F-FDG study, the number of animals per group was 4 for the C57BL/6J treated with BLM and also 4 for the C57BL/6J treated with saline (control group, imaged on day 1). For ^{64}Cu-GPVI-Fc experiments, the number of C57BL/6J per group was 9 for control (4 imaged on day 21 and 5 on day 28), 5 for 3 days, 9 for 7 days, 9 for 14 days, 7 for 21 days and 8 for 28 days post i.t. BLM deposition (p.d.). For ^{64}Cu-GPVI-Fc isotype experiment, 4 C57BL/6J mice were scanned at day 14 p.d.. For ethical reasons, animals presenting a weight loss of over 20% or showing significant signs of suffering were sacrificed and not included in the study.

Positron Emission Tomography (PET) and Magnetic Resonance Imaging (MRI)

For ^{18}F-FDG scans two mice were put on one bed facing each other to get the thorax of each mouse as close as possible together. High resolution PET scans were performed using Inveon

small-animal PET scanners (Siemens Healthcare, Erlangen, Germany) with Inveon Acquisition Workplace Version 2.1.272 Software (Siemens Medical Solutions, Knoxville TN 37932, USA). Tracers (one per animal group) were injected intra venously with an activity of 12±1.2 MBq per mouse. ^{18}F-FDG was injected 5 s after the start of a 1 h dynamic scan followed by an 827 s transmission scan. ^{64}Cu -GPVI-Fc was imaged with a 10 min static scan 3 h, 24 h and 48 h post tail-vein injection. Each PET scan was followed by two MRI sequences for anatomical reference using a 7-T small-animal scanner (ClinScan; Bruker Biospin MRI GmbH, Ettlingen, Germany) with the Paravision 6.0.1 Software (Bruker Corporation, Billerica MA 01821, USA): T2-TurboRARE (echo/repetition time: 30.82/600 ms; echo spacing: 5.137 ms; rare factor: 16; slice thickness 23 mm; image size: 256x128x92, field of view: 64x32x23 mm) and T1-FLASH-3D sequence (1 mouse bed: echo/repetition time: 3/12 ms; flip angle: 8.9°; slice thickness: 23 mm; image size: 256x128x92; field of view: 64x32x23 mm | 2 mice bed: echo/repetition time: 3/11 ms; flip angle: 5°; slice thickness: 21.12; image slice: 272x136x96; field of view: 60x30x21.12 mm). Mice were put under 1.5% isoflurane anesthesia in 100% O_2 at 1.5 L/min during all scans and body temperature was kept at 37°C using warming pads. PET images were reconstructed with OSEM3D SP function (spatial resolution of 1.4 mm, axial field-of-view: 12.7 cm and trans-axial field-of-view: 10 cm) and analyzed with Inveon Research Workplace software (Siemens Healthcare) using fiducial markers containing a low concentration of radiotracer for spatial co-registration with MRI. Regions of interest (ROI) were drawn manually for left and right lung lobes independently using the MR image as a spatial marker. For the ^{64}Cu-GPVI-Fc experiments quantification, particular care was taken to segment the lungs based on anatomical MRI images and avoid spillover from the heart. For the dynamic ^{18}F-FDG PET scans only the right lobes of the lung were taken into account for quantification. The left side was excluded to avoid spill over due to high tracer uptake of the heart muscle and consequently strong

partial volume effect in the surrounding lobes. Decay corrected mean activity (Bq/cc) in ROI was normalized to injected dose (ID) of tracer to get %ID/cc. ^{18}F-FDG mean uptake value was obtained from dynamic PET scan data obtained after tail-vein injection. The ^{64}Cu-GPVI-Fc ID values were obtained from 10 min static PET scans.

Biodistribution

1 mL reference activity tubes were prepared from a solution containing 240±24 MBq/L of radiotracer in water. After the last scan retro bulbar blood sampling was performed under 1.5% isoflurane anesthesia in 100% O_2 before sacrificing the mice using CO_2. The abdomen and thorax of mice were opened, the abdominal aorta was cut open and mice were perfused with 20 mL 4°C phosphate buffered saline through the right ventricle. The following organs were taken to measure radioactive counts per minute (CPM) *ex vivo*: blood, heart, entire lung, right liver lobe, spleen, right kidney, intestines and left upper leg muscle. Measurement tubes with reference activities and organs were put into a 2480 Automatic Gamma Counter, WIZARD$^{2®}$ from PerkinElmer (Waltham, Massachusetts, USA). CPM from reference tubes and weight of organs were used to calculate decay corrected *ex vivo* activity as %ID/g. Lungs were fixated with 4.5% paraformaldehyde (PFA) for 24 h and afterwards embedded into paraffin for preparation for histology experiments.

Histology

After imaging, mice were sacrificed and perfused as described before and lungs were fixated in 4.5% formalin (SAV Liquid Production GmbH, 83126 Flintsbach am Inn, Germany) and embedded in paraffin. Afterwards, paraffin embedded lungs were cut into 5 µm thick slices using a microtome (Leica, Wetzlar, Germany) and stained with hematoxylin and eosin (H&E) and Masson trichrome (MT). All samples were scanned with the Nanozoomer (Hamamatsu) and

processed with the programs Case Viewer and Adobe Photoshop CS6. Photomicrographic images were acquired with an Axioskop 2 plus Zeiss microscope equipped with a Jenoptik (Laser Optik System, Jena, Germany) ProgRes C10 plus camera and software. Final image preparation was performed with Adobe Photoshop CS6. Scoring of inflammation was performed based on H&E as follows: 0 (no inflammation), 1 (mild inflammation), 2 (moderate inflammation) and 3 (prominent inflammation). Fibrosis scoring was done following the modified Ashcroft scale (*4*). For C57BL/6J mice 5 mice from control, 7, 14 and 21 days and 4 mice from 3 and 28 days were used for histological scoring.

For fluorescence microscopy, flash-frozen lung slices were stained with different primary antibodies for ECM fibers: anti-fibronectin (Abcam, Cambridge, United Kingdom, # ab23750), anti-fibrinogen (DAKO, Jena, Germany, # F 0111), anti-collagen I (Abcam, # ab34710), anti-collagen II (Abcam, # ab34712) or anti-collagen III (Abcam, # ab7778). For secondary antibody anti-rabbit Cy3 (Dianova, Hamburg, Germany, # 711-166-152) was used to visualize ECM fibers and anti-human IgG-Cy5 (Dianova, Hamburg, Germany, #709175149) was used to visualize NOTA-GPVI-Fc. Nuclei were stained using YO-PRO-1 (Molecular Probes, # Y3603) and images were acquired using a Zeiss LSM 800 system (Carl Zeiss, Oberkochen, Germany) with ZEN 2.3 (blue edition) software (Carl Zeiss Microscopy GmbH, Jena, Germany).

Data Evaluation and Statistics

Statistical analysis was performed using Ordinary one-way ANOVA (Multiple comparison test based on Dunnett's correction) in GraphPad Prism 9.0.1 for comparison of lungs at different time points, groups were compared to respective control. For *ex vivo* biodistribution comparison of different organs mixed-effects analysis was used, groups were compared to respective control. For comparison between uptake of ^{64}Cu -GPVI-Fc and radiolabeled isotype control unpaired t-

test was used. For histological scoring evaluation two-way ANOVA was used. Significant results are depicted in figures using * ($P \leq 0.05$), ** ($P \leq 0.01$), *** ($P \leq 0.001$) and **** ($P \leq 0.0001$) for Ordinary one-way ANOVA (*in* and *ex vivo* uptake of lungs at multiple time points or different tracer compared to a control) and two-way ANOVA (Mixed-effect analysis) (*ex vivo* biodistribution of PET-tracer in different organs at multiple time points compared to control). Static uptake results show each individual data point together with the mean of each group and its standard deviation. γ-counter results from mice (n=3) in the ^{18}F-FDG study was identified as outlier by Grubb's test, as results from a user error during *ex vivo* uptake measurement, and removed from further statistical *ex vivo* evaluation.

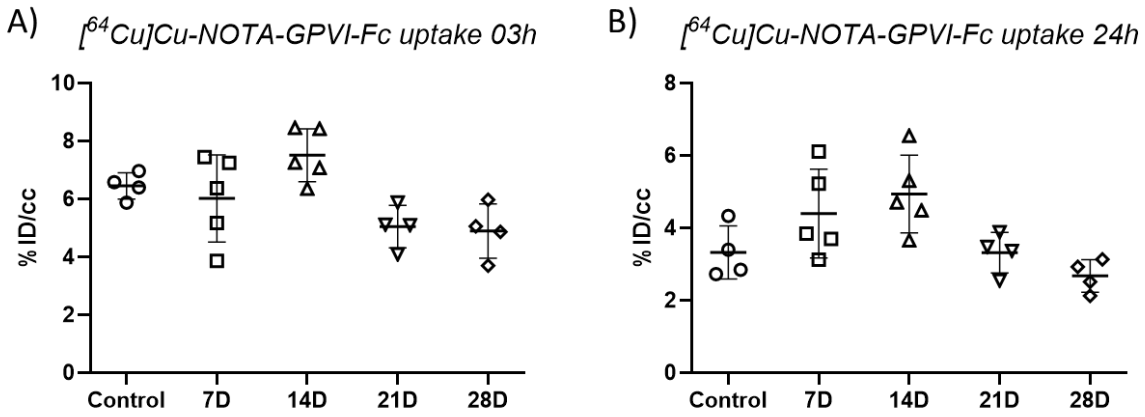

Supplemental Figure 1: *In vivo* ^{64}Cu-NOTA-GPVI-Fc (^{64}Cu -GPVI-Fc) uptake 03 (A) and 24 h (B) post tracer injection. No significant increase was seen for both scan times according to Ordinary one-way ANOVA.

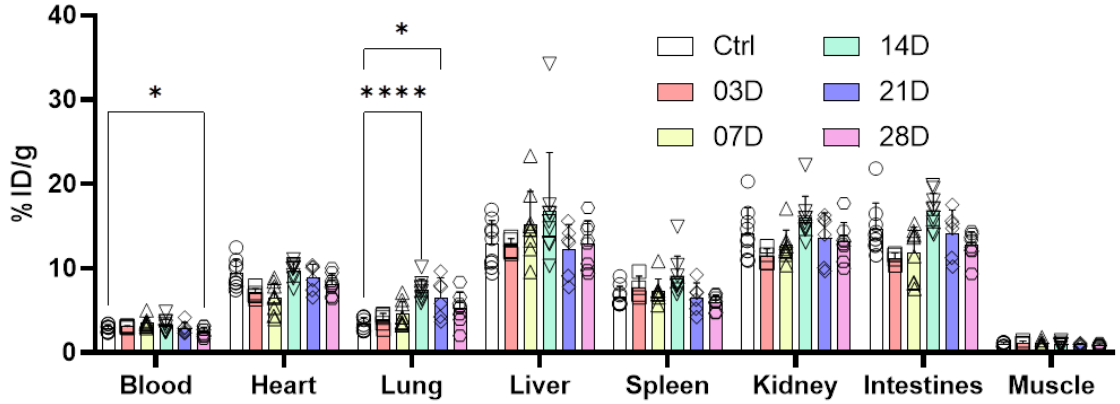

Supplemental Figure 2: *Ex vivo* biodistribution of ^{64}Cu -NOTA-GPVI-Fc [%ID/g] in main organs in control animals or at various days after bleomycin deposition in C57BL/6J mice.

P values are indicated for Mixed-effect analysis (biodistribution *ex vivo*) using * ($P \leq 0.05$), ** ($P \leq 0.01$), *** ($P \leq 0.001$) and **** ($P \leq 0.0001$).

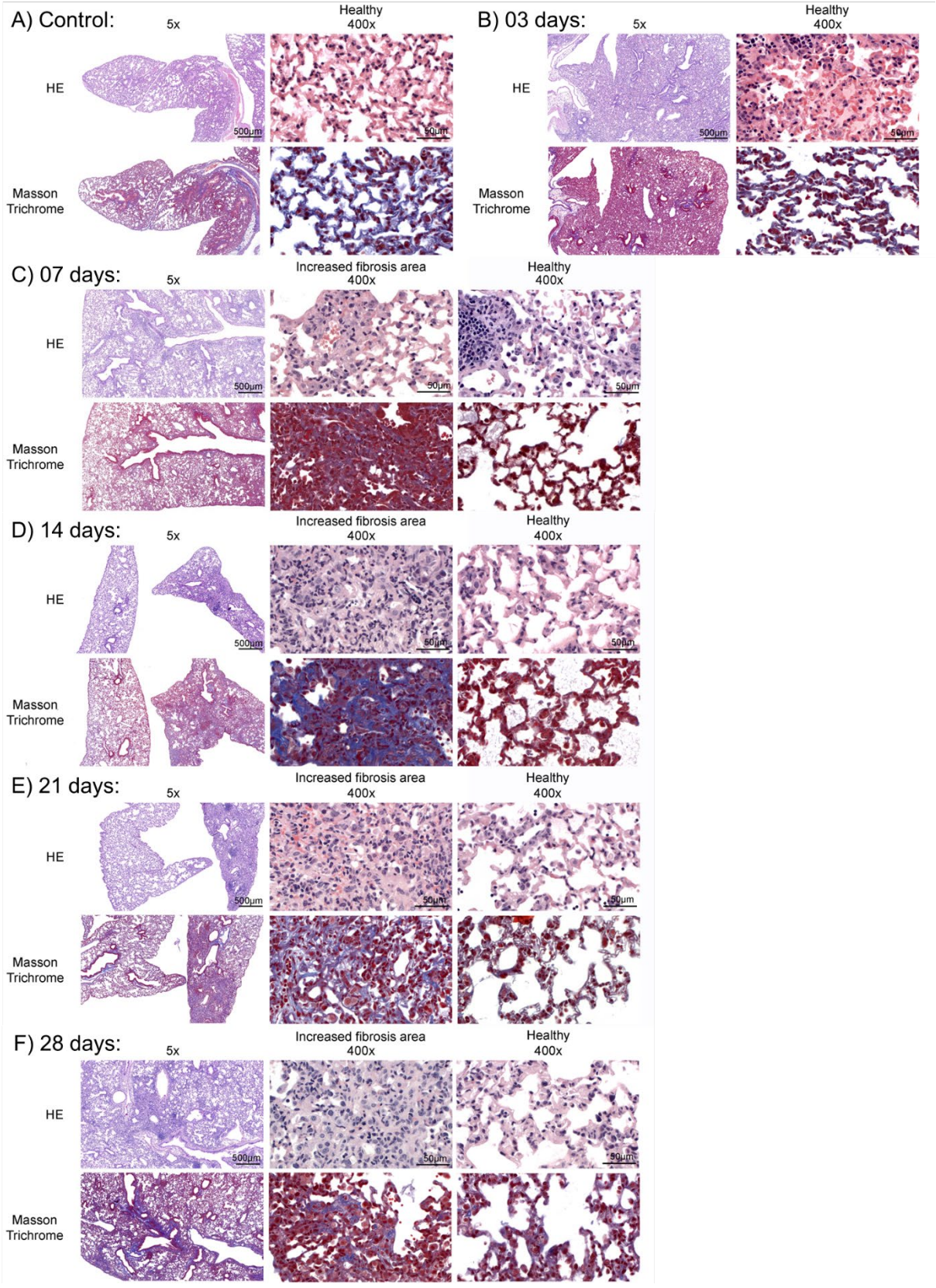
A) Control:
5x
Healthy
400x
HE
Masson
Trichrome
500µm
50µm
B) 03 days:
5x
Healthy
400x
HE
Masson
Trichrome
500µm
50µm
C) 07 days:
5x
Increased fibrosis area
400x
Healthy
400x
HE
Masson
Trichrome
500µm
50µm
D) 14 days:
5x
Increased fibrosis area
400x
Healthy
400x
HE
Masson
Trichrome
500µm
50µm
E) 21 days:
5x
Increased fibrosis area
400x
Healthy
400x
HE
Masson
Trichrome
500µm
50µm
F) 28 days:
5x
Increased fibrosis area
400x
Healthy
400x
HE
Masson
Trichrome
500µm
50µm

1

Supplemental Figure 3: Hematoxylin & eosin (HE) and Masson trichrome staining of control and PF C57BL/6J lungs. Representative lungs for each time-point. The control (A) showed completely healthy lung tissue and 3 days post deposition (p.d.) (B) showed no sign of fibrosis, but small signs of inflammation. In the mouse 7 days p.d. (C) clear signs of inflammation were visible as well as small fibrotic areas. At day 14 p.d. (D) fibrotic foci were most prominent. A small reduction of fibrotic areas was visible on day 21 p.d. (E) in comparison to day 14 p.d. On day 28 p.d. (F) further reduction of fibrosis was visible.

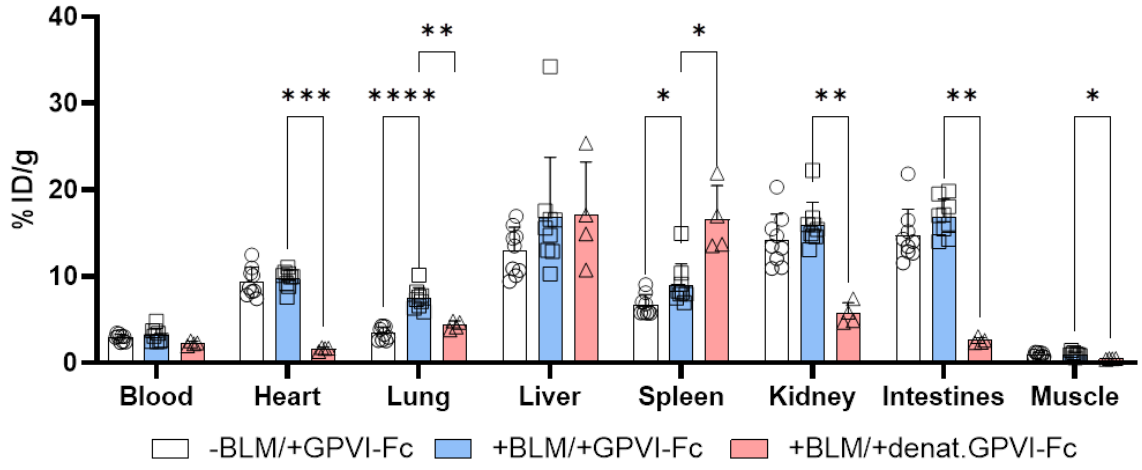

Supplemental Figure 4: *Ex vivo* biodistribution of naïve ^{64}Cu-NOTA-GPVI-Fc (^{64}Cu-GPVI-Fc) and denatured ^{64}Cu-GPVI-Fc (Isotype) [%ID/g] in main organs in control animals or14 days after bleomycin deposition in C57BL/6J mice. P values are indicated for Mixed-effect analysis (biodistribution *ex vivo*) using * ($P \leq 0.05$), ** ($P \leq 0.01$), *** ($P \leq 0.001$) and **** ($P \leq 0.0001$).

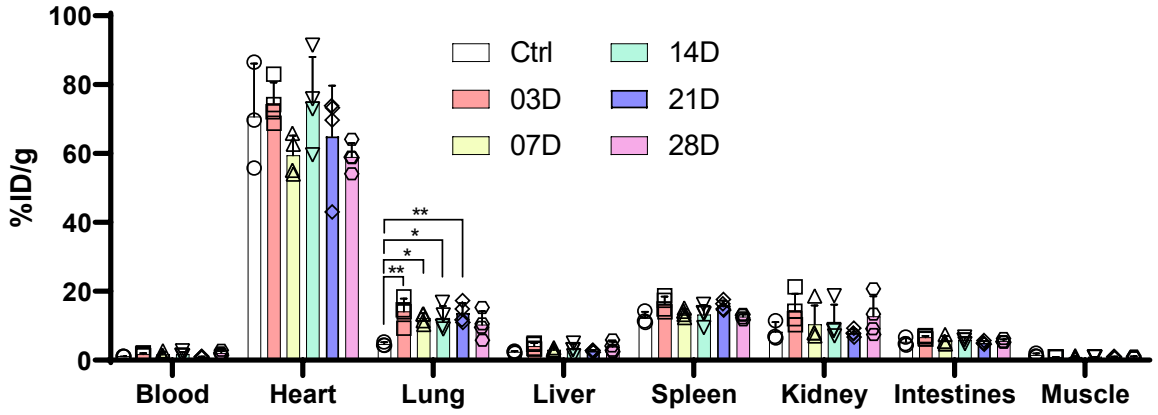

Supplemental Figure 5: ***Ex vivo*** **biodistribution of ^{18}F-FDG [%ID/g] in main organs in control animals or at various days after bleomycin deposition in C57BL/6J mice.**

Supplemental Table 1: Comparison of ^{18}F-FDG uptake *in vivo* versus blood glucose level.

Individual uptake values normalized to injected dose (ID) per cubic centimetre (cc) for all animals; values were compared to blood glucose levels measured before PET scan. No correlation between ^{18}F-FDG uptake and blood glucose level was visible. (p.d.: post deposition)

Group	Lung uptake (%ID/cc)	Blood glucose (mg/dL)
Control	4.53	174
	5.39	177
	4.45	160
	4.31	141
3 days p.d.	6.58	187
	8.57	161
	8.34	170
	7.58	148
7 days p.d.	7.87	227
	8.6	194
	7.62	166
	7.21	166
14 days p.d.	6.18	224
	9.24	175
	6.32	187
	7.82	213
21 days p.d.	7.16	236
	6.67	248
	6.37	202
	6.76	175
28 days p.d.	7.77	256
	5.27	244
	8.35	182
	7.46	198

REFERENCES

1. Beziere N, Fuchs K, Maurer A, et al. Imaging fibrosis in inflammatory diseases: targeting the exposed extracellular matrix. *Theranostics.* 2019;9:2868-2881.

2. Akazawa-Ogawa Y, Nagai H, Hagihara Y. Heat denaturation of the antibody, a multi-domain protein. *Biophys Rev.* 2018;10:255-258.

3. Walters DM, Kleeberger SR. Mouse models of bleomycin-induced pulmonary fibrosis. *Curr Protoc Pharmacol.* 2008;Chapter 5:Unit 5 46.

4. Hubner RH, Gitter W, El Mokhtari NE, et al. Standardized quantification of pulmonary fibrosis in histological samples. *Biotechniques.* 2008;44:507-511, 514-507.